Benchmarking the Electrochemical CO_2 Reduction on Polycrystalline Copper Foils The Importance of Microstructure Versus Applied Potential

Asperti, Simone; Hendrikx, Ruud; Gonzalez-Garcia, Yaiza; Kortlever, Ruud

DOI
10.1002/cctc.202200540

Publication date
2022

Document Version
Final published version

Published in
ChemCatChem

ChemCatChem

Research Article
doi.org/10.1002/cctc.202200540

Chemistry Europe
European Chemical Societies Publishing

www.chemcatchem.org

Special Collection

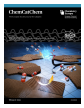

Benchmarking the Electrochemical CO_2 Reduction on Polycrystalline Copper Foils: The Importance of Microstructure Versus Applied Potential

Simone Asperti,[a] Ruud Hendrikx,[b] Yaiza Gonzalez-Garcia,[b] and Ruud Kortlever*[a]

Copper is one of the most promising catalysts for the CO_2 reduction reaction (CO_2RR) due to its unique capability of producing multicarbon products in appreciable quantities. Most of the CO_2RR research efforts have been directed towards the development of new electrocatalysts to either increase product selectivities or decrease overpotentials. In contrast, only a few studies have systematically tested or benchmarked CO_2RR performances of electrocatalysts. In this paper, for the first time, the performances of five different polycrystalline copper foils purchased from different suppliers are benchmarked for their CO_2RR performance. Their differences are characterized in terms of microstructural features and the effect that these microstructural properties have on the electrocatalytic behavior during potentiostatic CO_2RR experiments are evaluated. It is shown that the potential applied is the dominant factor controlling CO_2RR selectivities, leading to the conclusion that microstructural properties of polycrystalline copper electrodes have a negligible effect on the outcome of CO_2RR experiments.

Introduction

Many technologies have been proposed to reduce the rising CO_2 concentrations in the atmosphere. One promising approach is the electrochemical conversion of CO_2 to fuels and bulk chemicals, where CO_2 captured from the atmosphere can for instance be converted into hydrocarbons such as methane and ethylene, utilizing electricity provided by renewable sources.[1] This process can be conducted on a plethora of different electrocatalysts, including metallic foils, nanostructured materials, metal-organic catalysts, and multimetallic electrocatalysts.[2] Among them, copper-based materials are the only electrocatalysts capable of producing hydrocarbons in appreciable quantities.[3] Nevertheless, the selectivity of the reaction towards one specific product remains low, and the overpotentials for the production of hydrocarbon products remain relatively high.[4]

Most of the CO_2 reduction reaction (CO_2RR) research efforts have therefore been directed towards developing new electrocatalysts to either increase product selectivities or decrease overpotentials. Only a few studies have systematically tested or benchmarked the CO_2RR performances of electrocatalysts. For copper specifically, Kuhl et al. investigated the CO_2RR on a polycrystalline copper foil acquired from Sigma–Aldrich and mapped its product selectivity as a function of the applied potential.[1a] The authors used a compression H-cell with a high electrode surface area to electrolyte volume ratio that allowed for accurate product analysis. This resulted in the detection of 16 different products. The study also highlights the potential dependency of the electrocatalytic process: the highest faradaic efficiencies (FEs) for compounds with more than one carbon atom fall between −0.80 and −1.20 V vs. RHE. This potential dependency was also shown on Alfa–Aesar polycrystalline copper foils, where the four major gaseous products – hydrogen, carbon monoxide, methane and ethylene – were investigated using a substantially different setup[1a,5] . The aforementioned studies do not consider the influence of the microstructural properties of the polycrystalline copper foils on the efficiency and selectivity of CO_2RR. In contrast, Shibata et al. observed clear differences in CO_2RR product distributions when comparing the electrocatalytic performance of polycrystalline copper foils acquired from Eurofysica and Alfa–Aesar.[6] Shibata et al. associated the observed differences with differences in the crystallographic orientation of surface atoms, as well as the presence of different copper oxides on the electrode surface.

From a thermodynamic point of view, there are remarkable differences between Cu(100), Cu(111) and Cu(110) surfaces. The different coordination number of copper surface atoms in each configuration modifies their surface energies and, in turn, the binding energy between CO_2RR intermediates and the copper surface. For example, the highest binding energy values are found on Cu(110), whilst the lowest are found on Cu(111).[2c]

[a] S. Asperti, Dr. R. Kortlever
Department of Process & Energy, Faculty of Mechanical, Maritime and Materials Engineering,
Delft University of Technology,
Leeghwaterstraat 39, 2628 CB, Delft (The Netherlands)
E-mail: R.Kortlever@tudelft.nl

[b] Dr. R. Hendrikx, Dr. Y. Gonzalez-Garcia
Department of Materials Science and Engineering,
Faculty of Mechanical, Maritime and Materials Engineering,
Delft University of Technology
Mekelweg 2, 2628 CD, Delft (The Netherlands)

Supporting information for this article is available on the WWW under https://doi.org/10.1002/cctc.202200540

Special Collection

This publication is part of a joint Special Collection with EurJOC and EurJIC on the Netherlands Institute for Catalysis Research. Please see our homepage for more articles in the collection.

Moreover, a preferential multicarbon pathway for CO_2RR has been observed on Cu(100) surfaces that drives the reaction selectivity to multicarbon products, while Cu(111) surfaces lead to higher selectivities for methane production.[7] This is assumed to be caused by geometrical reasons: in the case of Cu(111) the distance between two adsorbed CO molecules is too low for CO-dimerization, whereas, with Cu(100) the distance between two adsorbed CO molecules is closer to the distance between two carbon atoms in an ethylene molecule, thereby facilitating C–C bond making.[8] Moreover, the selectivity of copper catalysts for CO_2RR has been shown to depend on grain sizes, grain boundary densities and the micro-strain of the surface. On copper electrodes, a linear relationship between the partial current density towards CO production (j_{CO}) and the surface grain sizes has been found,[9] as well as a relationship between the ethylene selectivity and the grain boundary density.[10] Conversely, on oxygen-derived copper electrodes, a linear relationship was found between the faradaic efficiency toward ethylene and crystallite sizes.[11]

Recent in-situ ATR-SEIRAS and Raman spectroscopy studies have helped to shed light on the role of the applied potential towards the formation of reaction intermediates and, in turn, the CO_2RR selectivity. For example, Katayama et al. conducted ATR-SEIRAS tests that clearly demonstrated CO_{ads} formation on the electrode surface taking place only at relatively high overpotentials.[12] This has been confirmed with in-situ Raman spectroscopy, regardless of the morphology of the catalyst structure.[13] On the other hand, Scholten et al.[14] showed that the catalyst surface preparation has a high impact on the CO_2RR selectivity, contradicting previous work on the effect of surface atom crystallographic orientations. Moreover, many studies have shown morphological changes of the (nanoparticulate) catalysts during CO_2RR, among them: Ostwald ripening, catalyst fragmentation and agglomeration, surface poisoning due to the formation of carbonaceous species and catalyst dissolution.[15] Raaijman et al. also showed that Cu(100) is the least stable facet in CO_2RR reaction conditions, while Cu(111) and Cu(110) tends to be more stable under pure cathodic conditions.[16]

These literature results raise the question whether microstructural properties play an important role in the performance of polycrystalline copper electrodes. While the effect of micro-strain, crystallite sizes, grain sizes and surface atom crystallographic orientation were individually demonstrated on copper catalysts, there is no scientific evidence about their synergic effects during the CO_2RR, as would be the case with polycrystalline copper foils. Alternatively, differences in CO_2RR performance of polycrystalline copper foils tested in the literature can be attributed to either differences in the microstructural properties of the polycrystalline copper foil or differences in electrochemical cell designs and experimental procedures. For instance, Yang et al. have emphasized the role of the cell configuration as cell geometry, membrane type, and electrode placement can have profound consequences in terms of CO_2RR selectivity.[17]

This work aims to benchmark the behaviour of different polycrystalline commercial copper foils for CO_2RR. At the same time, it aims to investigate whether the microstructural properties of these polycrystalline foils play an important role in electrocatalytic performance. The microstructural features of the commercial foils were first characterized, particularly the surface atom crystallographic orientations, micro-strain, crystallite size and grain sizes. The electrocatalytic performance of the foils was tested under potentiostatic conditions using a compression H-cell with a high surface area to volume ratio. In discussing our findings, we comment on the role of microstructure versus applied potential, showing clear evidence on which is more dominant in determining the outcome of the CO_2RR on polycrystalline copper foils.

Results and Discussion

Characterization of the Cu foils

Before every experiment, the copper foils were mechanically polished and electropolished, using a procedure similar to the procedure used by Kuhl et al.[1a] X-ray fluorescence (XRF) analyses (reported in Supplementary Information, Section S7) were conducted after electropolishing, showing high weight percentages of copper and low percentages of oxygen. This is similar to the results obtained with depth profiling X-ray photoelectron spectroscopy (XPS) performed on Mateck foils (Figure 1). Traces of C(1s) can be associated with adventitious carbon and traces of N(1s) are leftovers from the vacuum operation.

In light of these results, the elemental composition of the catalyst surface was constituted by mainly copper and copper oxides, and no impurities were detected. Knowing that copper oxides are thermodynamically unstable at the highly cathodic potentials applied during CO_2RR experiments, we can safely

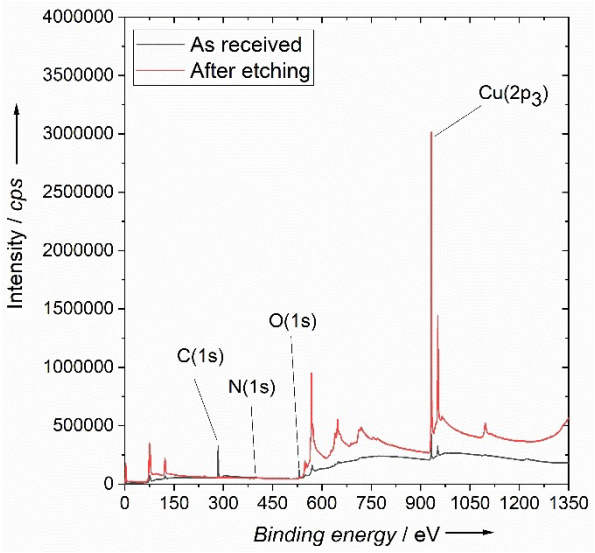

Figure 1. Depth profiling X-ray photoelectron spectroscopy results of Mateck foils. The spectrum in black was recorded on the sample as-received. The spectrum in red was recorded after removal of ca. 200 μm of the outermost atomic layers

assume that all of the copper oxides species must be converted to pure copper during the first minutes of electrolysis.[18]

X-ray diffraction (XRD) was used to investigate the crystallinity of the polycrystalline copper foils. To account for heterogeneities of the surface, five different areas of the foil were investigated (see Supplementary information, Figure S13). XRD peak area results show different crystallographic surface atom orientations for each copper foil purchased from a different supplier. The diffractograms are displayed in Figure 2 and the corresponding peak areas are reported in Figure S12.

Following previous literature studies, the peaks located at 45° can be assigned to Cu(111), at 50° to Cu(100) and 75° to Cu(110).[19] The highest peak for Cu(111) areas was recorded on the Goodfellow and Alfa–Aesar samples, whereas on the Mateck sample the Cu(111) peak is almost negligible. For Cu(100) the highest peak areas were obtained with Sigma–Aldrich, followed by Mateck, Alfa–Aesar, Goodfellow and Eurofysica. For Cu(110), however, the highest peak areas were found on Mateck foils, followed by Eurofysica, Goodfellow, Sigma–Aldrich and Alfa–Aesar. Interestingly, the Sigma–Aldrich diffractograms display remarkable differences in the Cu(100) peak intensity, differing significantly between the positions analyzed. As can be seen in Figure 2, the Cu(100) signal was relatively high in two spots investigated (position 2 and 4), but relatively low for the other positions considered. This underlines the high anisotropy of Sigma–Aldrich foils. The recorded signals for the other foils did not show substantial differences among the investigated spots.

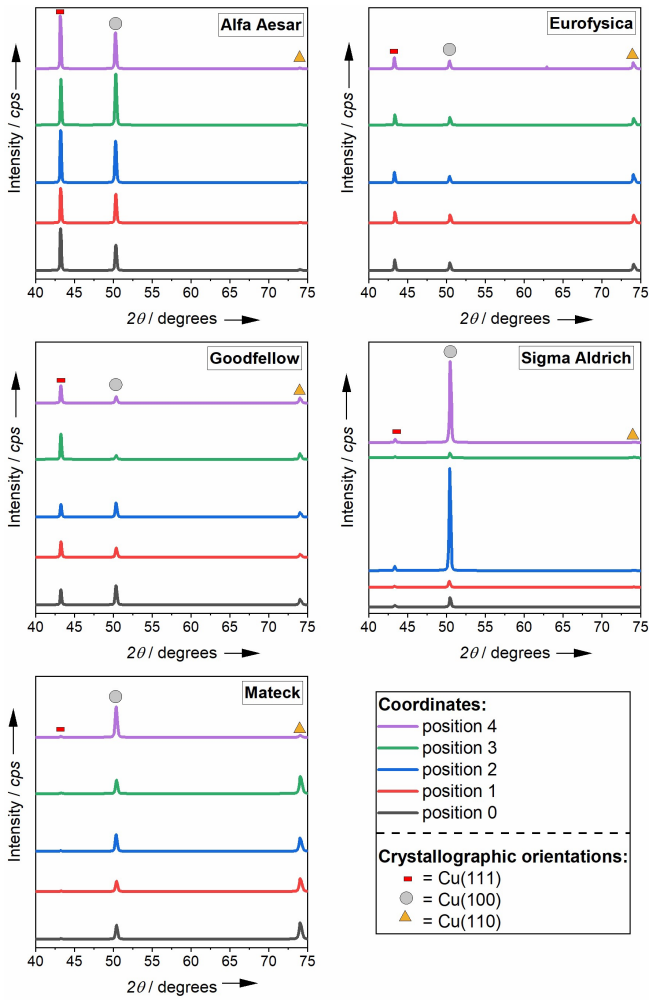

Figure 2. XRD diffractograms recorded for polycrystalline copper foils purchased from five different supplies. To account for heterogeneities of the foils five different regions of the sample surface were investigated

XRD peak broadenings were further analyzed to calculate the average crystallite sizes and the micro-strain values using the Scherrer equation (see Table 1). The smallest crystallite sizes are recorded on Mateck samples and the largest on Eurofysica. A different trend was observed in the case of micro-strain values. The lowest values were recorded on Alfa–Aesar foils, followed by Eurofysica, Goodfellow, Mateck and Sigma–Aldrich.

Two different electrocatalytic performances can be expected on the copper foils when solely considering the crystallographic orientations. First, a higher product selectivity towards ethylene production is expected on Sigma–Aldrich copper foils, due to their high Cu(100) peak areas.[20] Second, a higher selectivity for CO production is expected on Mateck foils due to the high peak areas of both Cu(110) and Cu(100)[21] . On the other hand, previous work on single crystal copper foils[8,20,22] suggests that Cu(100) favors the C_2 pathway, meaning that Mateck foils are also expected to have high selectivity towards multicarbon products. However, when considering mainly the crystallite sizes, based on the work of Handoko et al.,[11] the highest selectivities for CO production are expected on Sigma–Aldrich, whilst, on Eurofysica foils the CO selectivity should be the lowest.

The grain sizes of the copper samples were characterized by chemical etching of the surface and optical microscope imaging (see Figure 3). The averaged grain size values are reported in Table 2. There is a large variation in average grain sizes with the different foils. Sigma–Aldrich copper foils have the biggest and the most irregular grains with an elongated shape (Figure 3e). The high standard deviation recorded on Sigma–Aldrich foils (Table 2) also indicates its high anisotropy, in line with the XRD diffractogram results. Most likely, this could be a consequence

Table 1. Crystallite sizes (β) and micro-strain values (ε) recorded on each brand.

Brand	β [nm]	ε [%]
Sigma–Aldrich	62 ± 4	0.124 ± 0.006
Goodfellow	60 ± 4	0.059 ± 0.005
Alfa–Aesar	62 ± 5	0.017 ± 0.006
Eurofysica	87 ± 3	0.043 ± 0.006
Mateck	49 ± 5	0.093 ± 0.017

Table 2. Averaged grain sizes for each sample, with their standard deviation.

Brand	L [μm]
Sigma–Aldrich	240 ± 263
Goodfellow	39 ± 17
Alfa–Aesar	25 ± 22
Eurofysica	15 ± 5
Mateck	56 ± 30

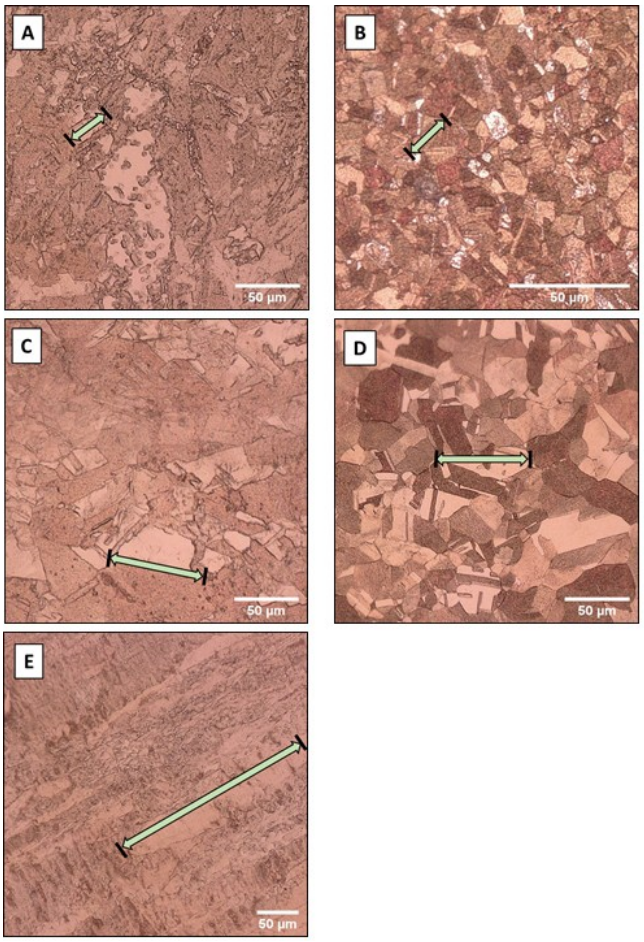

Figure 3. Representative optical microscope images after etching of a) Alfa–Aesar, b) Eurofysica, c) Goodfellow, d) Mateck, e) Sigma–Aldrich copper foils. The arrows indicate one representative grain length for each sample.

of a cold rolling process used during the industrial production of this brand.[23] On the other hand, Eurofysica samples showed the most regular pattern of grains, whose shape was found to be squared (Figure 3b). The averaged grain size value for the Eurofysica sample was the smallest among the samples analyzed. Mateck foils also displayed a regular pattern in terms of grain shape: their averaged sizes were almost four times bigger than Eurofysica. Instead, grains on Goodfellow foils were less distinguishable, and Alfa–Aesar did not show any clear grain shape pattern.

The grain boundaries density has been indicated to play a pivotal role during CO_2RR: the smaller the grain sizes, the higher the grain boundary density and the expected value of the j_{CO}.[24] Additionally, samples with a higher grain boundaries density are expected to show higher C_2 selectivities.[10] Therefore, considering the grain size values found in Table 2, Eurofysica foils are expected to show the highest j_{CO} (and in turn, the highest FE_{CO}), as well as the highest FE for multicarbon products, followed by Alfa–Aesar, Goodfellow, Mateck and Sigma–Aldrich, if grain size effects play an important role in determining the overall electrocatalytic activity.

Electrochemical analysis

The differences in the electrochemically active surface area of all copper foils were measured using double-layer capacitance measurements (see Supplementary information, Section S4). Cyclic voltammograms were recorded in the non-faradaic potential window between 0.12 and 0.18 V vs. RHE (see Supplementary information, Section S5). From the voltammograms reported in Figure S9, the average current values were collected at 0.16 V vs. RHE and plotted versus the sweep rates (w) (see Figure 4). The double-layer (C_{dl}) capacitance was calculated from the slopes in Figure 4, and their values are reported in Table 3.

The values for the actual electrochemically active surface area were not calculated since a reference sample is needed for comparison.[25] This has never been univocally reported for polycrystalline copper foils to the best of our knowledge. Nevertheless, the C_{dl} values are meaningful to underline the differences between the electrochemically active surface area for each sample involved. No significant differences in the double layer capacitance values were observed for the copper foils used. Therefore, we can conclude that the electrochemically active surface areas for the studied foils are very similar, regardless of the brand of copper foil.

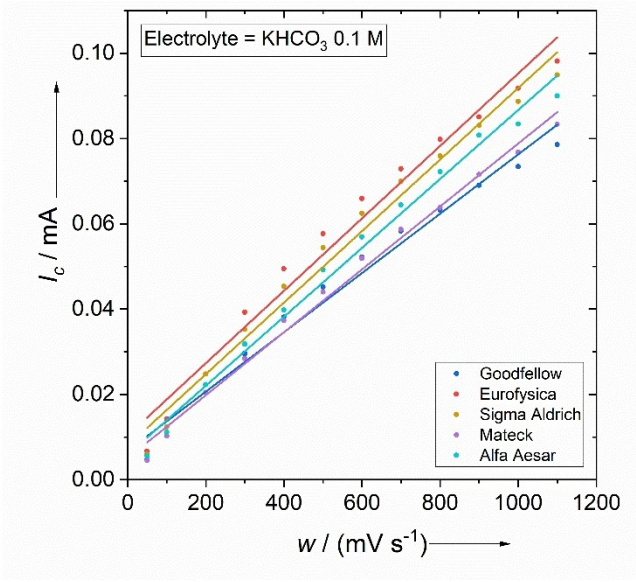

Figure 4. Average current values recorded at 0.16 V vs. RHE versus the sweep rate (w).

Table 3. Double-layer capacitance (C_{dl}) values recorded for every copper foil brand.

Brand name	C_{dl} [µF]
Sigma–Aldrich	84 ± 3
Goodfellow	70 ± 3
Alfa–Aesar	81 ± 3
Eurofysica	85 ± 5
Mateck	74 ± 2

Figure 5 shows the faradaic efficiencies for the CO_2RR products obtained with polycrystalline copper foils from different brands as a function of the applied potential. The values reported here are obtained from one-hour chronoamperometry experiments at a constant applied potential. Five different potentials were used for these experiments and error margins are given for variations in the faradaic efficiencies between reproduced experiments. Overall, the selectivities for multi-carbon products (ethylene, ethanol, 1-propanol and propionaldehyde) follow similar trends on each foil, with faradaic efficiencies increasing with more negative applied potentials. On the other hand, the selectivity for hydrogen production decreases with increasingly more negative applied potentials. For carbon monoxide production, the highest faradaic efficiencies were recorded at less negative applied potentials and decreased when the applied potential decreased. Instead, for methane production, the selectivity is very low at less negative applied potentials. From −1.0 V vs. RHE onwards an increase in methane selectivity is observed, reaching the highest faradaic efficiency for methane when the applied overpotential is the highest.

Different performances were observed for the other products. The faradaic efficiencies for formate production were the highest at −0.87 V vs. RHE for Mateck, Sigma–Aldrich and Alfa–Aesar foils. In contrast, for Goodfellow and Eurofysica foils, the peak in formate faradaic efficiency occurred at −0.97 V vs. RHE. In addition, acetaldehyde production was observed in a continuous potential range with Eurofysica foils, whereas, on other foils, its production was only observed at certain applied potentials. Other minor products, such as acetic acid, ethyl glycol and propionaldehyde, also followed irregular trends. For instance, acetic acid was exclusively produced by Mateck and Goodfellow copper foils at −1.03 V vs. RHE, and by Sigma–Aldrich foils at −1.15 V vs. RHE. Despite the low faradaic efficiency, ethylene glycol production could be observed only on Eurofysica at −1.06 V vs. RHE. Propionaldehyde, on the other hand, is observed at high applied overpotentials on all the samples studied, with the exception of Alfa–Aesar.

For Sigma–Aldrich, the above-mentioned results are similar to the results published by Kuhl et al.[1a] Furthermore, for Alfa–Aesar, the observed performances match the results of Karaiskakis et al., with the note that this work only reported the major gaseous CO_2RR products.[5] We should also note that the similarity between the results shown in Figure 5 and the results of Karaiskakis et al.[5] is not trivial, due to the fact that the cell design used by Kuhl et al.[1a] was similar to the one used in this paper,[26] but substantially different from the one used by Karaiskakis et al.[5] Nonetheless, the results shown in Figure 5e are considerably different from Shibata et al.[6] In their work, paraffins and olefins up to C_6 were observed, whereas in this work the longest hydrocarbon observed was 1-propanol. In addition, the above-mentioned authors showed a Schultz–Flory

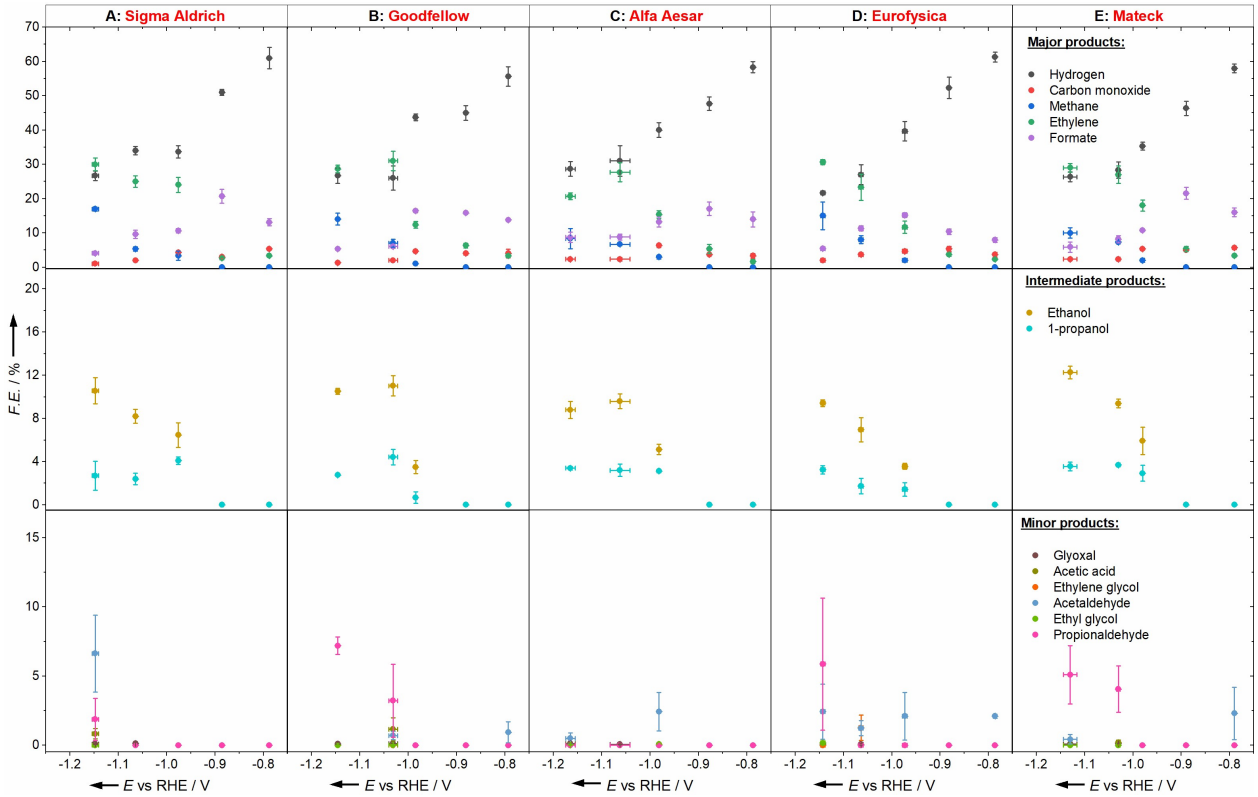

Figure 5. Faradaic efficiencies of products obtained during chronoamperometric CO_2RR measurements, with the potentials corrected for the ohmic drop, using a 0.1 M $KHCO_3$ electrolyte and polycrystalline copper foils from a) Sigma–Aldrich, b) Alfa–Aesar, c) Eurofysica, d) Goodfellow, e) Mateck foils. Results are reported as the average of three reproducible results, with their standard error.

distribution for the CO_2RR products,[6] whereas this is not the case in our work. Furthermore, Shibata et al.[6] operated under galvanostatic conditions, while in our study the faradaic efficiencies were determined under potentiostatic conditions.

The trends reported in Figure 5 are also not comparable to Chen et al.[10], where grain-boundary-rich copper samples were shown to perform better in terms of faradaic efficiencies for multicarbon products in a wide range of potentials from −1.0 to −1.3 V vs. RHE. In fact, in our study, the sum of the FEs for C_2 products was never close to 70%. A direct comparison between our research and Chen et al. cannot be made, due to the lack of information regarding grain sizes.[10] Moreover, the trends found here do not follow any linear relationships with micro-strain values, as was observed by Handoko et al.[11] The $FE_{ethylene}$-crystallite size relationship was reported under galvanostatic experiments,[11] while the potentiostatic experiments performed in the same study show similar trends to what we observe in Figure 5.

Although we discussed the effect that the microstructural features could have on the electrocatalytic properties of copper electrodes in the previous section, no clear differences in electrocatalytic behavior are observed for the copper foils studied here. Moreover, micro-strain, grains, crystallites, and the crystallographic orientation of surface atoms should not be considered independently in polycrystalline samples like the ones reported in our work. Nevertheless, the results reported Figure 5 show minor differences between the foils in terms of faradaic efficiencies. These minor differences in performance could be due to differences in the microstructural properties of the foils. However, the fact that each foil behaves similarly to any other brand investigated means that either there is no clear dominant effect of one feature with respect to another one or, when every microstructural feature is considered in a polycrystalline system, the overall synergistic effect is negligible. The reiteration of previous studies under potentiostatic conditions could also help to confirm and clarify the balance between CO_2RR performances and microstructure, as well as to further compare the results with similar experimental conditions.[6,10–11,27]

Despite the fact that the cell design used in this work operated with a lower CO_2 purge flow rate, with lower geometrical electrode surface areas and lower electrolyte volume[26] compared to the work of Kuhl et al.,[1a] the faradaic efficiency values recorded follow similar trends. This, once again, demonstrates the dominant role of the applied potential during CO_2RR. Most likely, the different parameters mentioned earlier might impact the mass transport limitations for CO_2RR reagents and products, explaining why small differences in performance are visible between this work and Kuhl et al.[1a] Furthermore, the dominant effect of the applied potential on the CO_2RR performance is in agreement with Kuhl's conclusions,[1a] where the CO_2RR pathways were described as potential dependent. Reiterating previous literature studies about the relationship between the microstructure and CO_2RR performance with a H-type cell and under constant potential conditions would help to improve the engineering of catalyst surfaces and, possibly, boost the CO_2RR performances towards the commercial interest.[6,10–11,27]

Conclusion

In this study, polycrystalline copper foils purchased from different suppliers were benchmarked for their CO_2RR performance. Differences in microstructural properties between each foil were observed, specifically relating to surface atom crystallographic orientations, micro-strain, crystallite sizes, and average grain sizes. No differences in surface purity and electrochemical surface area were observed between the samples. Following previous literature studies, trends in faradaic efficiencies for the copper foils were initially expected based on their differences in microstructural properties. Nevertheless, at the same applied potential, similar faradaic efficiency values were found independent of the foil that was used. This means that the potential applied during the electrolysis, is the dominant factor controlling the electrocatalytic performance, outperforming microstructural features and cell designs. While the role of microstructural features during CO_2RR was mostly evidenced under constant applied current, it would be helpful to reiterate these studies and also validate the results under potentiostatic conditions.

Experimental Section

Materials

Pure copper foils were purchased from five suppliers: Sigma–Aldrich (99.990% purity, USA), Goodfellow (99.999%, USA), Mateck (99.99%, Germany), Alfa–Aesar (99.999%, USA), Eurofysica (purity not declared, The Netherlands). For the characterization and CO_2RR, the used dimension for all the samples was 25 mm × 25 mm and 1 mm thickness.

For the execution of CO_2RR experiments, the in-line gas chromatograph (CompactGC 4.0, Global analyser solutions, The Netherlands) was calibrated with custom gas mixture cylinders containing different concentrations of the product gasses in CO_2 (Linde Gas Benelux B.V., The Netherlands) to obtain calibration curves for hydrogen, carbon monoxide, methane and ethylene in a concentration range from 50 to 8000 ppm.

The HPLC (Agilent Technologies 1260 Infinity, USA) was calibrated with standard aqueous disolutions in a range 0.1 mM to 50 mM with: oxalic acid (99%+, Sigma–Aldrich, USA), glyoxal (40% v% in water, Sigma–Aldrich, USA), formic acid (98%+, Sigma–Aldrich), acetic acid (99.9%+, Sigma–Aldrich, USA), ethylene glycol (99%+, Sigma–Aldrich, USA), acetaldehyde (99.5%+, Sigma–Aldrich, USA), methanol (99.9%+, Sigma–Aldrich, USA), ethanol (absolute, Sigma–Aldrich, USA), acetone (99.8%+, Sigma–Aldrich, USA), propionaldehyde (97%, Sigma–Aldrich, USA), 2-propanol (99.9%, Sigma–Aldrich, USA) and 1-propanol (99.9%, Sigma–Aldrich, USA).

The same chemicals were used for the calibration of the NMR (400 MHz Agilent, USA). To avoid NMR peak overlaps, two matrices were prepared in two different flasks and diluted with 0.1 M bicarbonate aqueous solution. The matrices contained respectively formaldehyde, formic acid, allyl alcohol, methanol, acetone, propionaldehyde, ethanol, 2 propanol (denominated as matrix A)

and acetaldehyde, ethyl acetate, ethylene glycol and n-propanol (denominated as matrix B), as well as phenol (99%+, Sigma–Aldrich, USA) and DMSO (99.9%+, Sigma–Aldrich, USA) as internal standards. The content of the compounds contained in each matrix was kept at 50 mM as concentration for each component within the two matrices, apart from phenol and DMSO whose concentration was kept fixed at 15 and 10 mM, respectively. Other standard solutions in a range from 10 to 0.05 mM were prepared accordingly from the 50 mM matrix A and B solutions, while maintaining a fixed concentration of Phenol and DMSO at 15 and 10 mM, respectively.

Surface pretreatment

The copper foils were first mechanically polished to a mirror-like finish. Copper foils were attached to a cylindric sample holder using bi-adhesive tape and manually sanded using P80, P180, P320, P800, P1200 and P2000 silicon carbide sanding paper (Struers, USA) on a rotating sanding machine (Labopol-21, Struers, USA). Then, copper foils were polished with a 3 μm diamond-based suspension (DiaDuo-2, 3 μm. Blue. 500 ml, Struers, USA) and 1 μm diamond-based suspension (DiaDuo-2, 1 μm. White. 500 ml, Struers, USA) on a rotating machine (Labopol-21, Struers, USA), using respectively Mol (Struers, USA) and Nap (Labopol-21, Struers, USA) as polishing cloth. Copper foils were then detached from the sample holder, washed abundantly with isopropanol and dried with a stream of hot air. Such stream was directed to the foils as much parallel to the sample surface as possible, in order to rapidly remove isopropanol from the polished surface. More specific information on the mechanical polishing is available in Supplementary Information, Section S9.

Afterwards, every copper sheet underwent a two-step electropolishing treatment to eliminate impurities and smoothen the surface. The copper sample was used as the anode, a graphite rod (99.999% purity, Strem Chemicals Inc., UK) as the cathode and the two components were immersed in an H_3PO_4 85% w/w solution (Sigma–Aldrich, USA). A potential of +2.1 V (vs. the graphite rod) was applied for 8 minutes. At the end of the treatment, the copper foils were washed thoroughly with ultrapure water, obtained with an ultrapure water purification system (MilliQ EQ 7000, Merck–Millipore, USA) equipped with a water treatment filter (0.22 mm, Merck–Millipore, USA), and then dried with a N_2 stream. This treatment was repeated twice before every experiment.

Surface characterization

The surface purity was determined with two different techniques: X-ray fluorescence spectrometry (XRF) and depth profiling X-ray photoelectron spectroscopy (XPS). XRF measurements were carried out using a WD-XRF spectrometer (Axios Max, Panalytical, UK), and data evaluation was done with SuperQ5.0i/Omnian software (Axios Max, Panalytical, UK). Depth profiling XPS measurements were carried out with K-Alpha XPS (ThermoFisher, USA), and data evaluation was done with the software CasaXPS. Depth profiling XPS was executed with an ion-gun operating at 2000 V in a four-steps-sequence, to remove ca. 200 μm of the outermost sample layers.

The differences in electrochemical surface area (ECSA) were measured using cyclic voltammetry.[14] In an H-type cell, cyclic voltammograms were recorded for each sample in a potential window comprised between −0.12 and $-0.18\ V_{RHE}$ at different sweep rates using a Biologic VSP-200 multichannel potentiostat (Biologic Science instruments, France) (see Supplementary information, Section S5). The averaged currents recorded were then plotted versus the sweep rate (w) and the capacitance values were determined from these plots.

Crystallographic orientation, crystallite sizes and micro-strain were estimated by X-ray diffraction (XRD) analysis. Electropolished samples were investigated with an D8-Lynxeye XRD-diffractometer (Bruker, USA), coupled with an Eiger-2 500k 2D-detector (Bruker, USA) using a Cu Kα 1 uS microfocus tube (Incoatec, Germany) as the source. The acceleration voltage was set at 50 kV and the probe current at 1000 μA. Besides, a UBC 0.5 mm collimator scatter screen was equipped with a uMC 1516 sample stage (Bruker, USA). The peak area and the peak width were extrapolated using Diffrac-Suite EVA (Bruker, USA). The crystallite sizes and the micro-strain value were estimated using the Scherrer equation.

Grain sizes were determined by means of chemical etching and optical microscopy. The etchant solution consisted of 8 g of $FeCl_3$ (97%, Sigma–Aldrich, USA), diluted in 100 mL of ultrapure water, combined with 25 mL of a 38% HCl solution (Sigma–Aldrich, USA) and was stirred for 20 minutes before use. The copper electrodes were immersed and etched for 40 seconds in the above-mentioned etchant, then washed with isopropanol. The etched samples were analysed with an optical microscope (VHX, Keyence, America) coupled with 250X–2500X lenses (VHX-$>$Z25UR), and the images were post-processed with ImageJ software (National Institute of Health, USA). The size of a total of 40 grains were measured and averaged along with their standard deviation.

Pre and post-mortem catalyst surface characterizations were conducted by means of a scanning electron microscope (Jeol JSM-6500F, Japan) coupled with an energy-dispersive X-ray spectrometry detector (Ultradry, Thermofischer, USA). The SEM was set to operate at an acceleration voltage of 15 kV and at a working distance of 25 mm.

CO_2RR experiments

The electrochemical reduction of CO_2 was conducted in a PEEK H-type cell similar to the cell design of Lobaccaro et al.[26] Before use, the cell was cleaned with a 20 v% nitric acid solution and washed thoroughly with ultrapure water before every experiment. The electropolished copper foils were used as the working electrode, while a platinum foil (25×25 mm, 0.1 mm thickness, 99.9%, Mateck, Germany) was cut in equal pieces of 25×25 mm and used as the counter electrode. A miniaturized leakless Ag/AgCl reference electrode (40 mm length, Innovative instrument, USA), stored in a freshly prepared KCl 3.5 M solution and controlled very carefully before every experiment (see Supplementary information, Section 1.3), was placed in the catholyte chamber and used to control the cathode potential. The catholyte and anolyte chambers were separated by an anion-exchange membrane (ForBlue Selemiom AMVN, AGC Engineering, Japan), which was replaced before every experiment and stored in utlrapure water. Both catholyte and anolyte chambers were filled up with 1.8 ml of a freshly prepared 0.1 M $KHCO_3$ aqueous electrolyte (Sigma–Aldrich, USA). During the experiment, CO_2 was purged from the bottom of the cell through the catholyte solution at flow rate of 8 nmL min^{-1}. In addition, the catholyte compartment was purged for at least 15 min with CO_2 before the measurement started at the same flow rate, to achieve CO_2-saturated bicarbonate solution conditions. The catholyte compartment was connected to an in-line gas chromatograph (CompactGC 4.0, Global analyser solutions, The Netherlands).

The CO_2RR measurements were carried out potentiostatically at five different applied potentials from −0.80 to −1.20 V vs. RHE. The potential was applied for 1 h using a Biologic VSP-200 multichannel potentiostat (Biologic Science Instruments, France). The cell resistance was measured by potentiostatic electrochemical impedance

spectrometry (PEIS) at E_{app} equal to E_{drift}. A representative plot is reported in Figure S1.2 in the supplementary information. The ohmic drop value was corrected for 85% and used as correction during CO_2RR. The remaining 15% was corrected manually, averaging the currents recorded throughout the whole CO_2RR process.

The faradaic efficiencies for gaseous products were determined in a reaction time interval comprised between 42 min and 54 min, while aliquots of the electrolyte were collected at the end of CO_2RR experiments to determine the faradaic efficiencies of liquid products. The liquid phase products were analyzed and quantified by HPLC (Agilent Technologies 1260 Infinity, USA), equipped with the built-in software OpenLab Control Panel, and NMR (400 MHz Agilent, USA), equipped with the built-in software OpenVnmrJ (University of Oregon, USA). For HPLC analysis, 5 μL of the catholyte solution was injected on two Aminex HPX-87H columns (Biorad) placed in series. The columns were heated to 60 °C, using an eluent containing 1 mM H_2SO_4 in ultrapure water and a refractive index detector (RID) for the detection of products. Formate, glyoxal, acetic acid, ethanol, 1-propanol and ethylene glycol were quantified with HPLC. For NMR measurements, 630 μL of the catholyte solution was mixed with 70 μL D_2O (99.9 atom% D, Sigma–Aldrich, USA) and 30 μL of a freshly prepared mixture containing 50 mM phenol (Sigma–Aldrich, USA) and 10 mM DMSO (Sigma–Aldrich, USA) as internal standards. NMR tubes (5 mm, Norell Select, USA) were employed to contain the solution. Since acetone was used to clean the NMR tubes, its quantification was not considered. Acetaldehyde, ethyl glycol, 2-propanol and propionaldehyde were quantified with NMR. An NMR water suppression procedure was performed on the post-CO_2RR samples, in order to get clearer spectrum (see Supplementary information, Section 10–12).

Acknowledgements

This activity is co-financed by Shell and a PPP-allowance from Top Consortia for Knowledge and Innovation (TKI's) of the Ministry of Economic Affairs and Climate in the context of the TU Delft e-Refinery program. The authors would also like to thank Bart Boshuizen for conducting X-ray photoelectron spectroscopy measurements.

Conflict of Interest

The authors declare no conflict of interest.

Data Availability Statement

The data that support the findings of this study are available from the corresponding author upon reasonable request.

Keywords: electrocatalysis · CO_2RR · microstructure · polycrystalline copper · applied potential

[1] a) K. P. Kuhl, E. R. Cave, D. N. Abram, T. F. Jaramillo, *Energy Environ. Sci.* **2012**, *5*; b) G. Centi, E. A. Quadrelli, S. Perathoner, *Energy Environ. Sci.* **2013**, *6*; c) A. Guan, Z. Chen, Y. Quan, C. Peng, Z. Wang, T.-K. Sham, C. Yang, Y. Ji, L. Qian, X. Xu, G. Zheng, *ACS Energy Lett.* **2020**, *5*, 1044–1053; d) X. Zhu, Y. Li, *WIREs Comput. Mol. Sci.* **2019**, *9*.
[2] a) J. He, Y. Li, A. Huang, Q. Liu, C. Li, *Electrochem. Energy Rev.* **2021**, *4*, 680–717; b) R. Kortlever, J. Shen, K. J. P. Schouten, F. Calle-Vallejo, M. T. M. Koper, *J. Phys. Chem. Lett.* **2015**, *6*, 4073–4082; c) M. K. Birhanu, M.-C. Tsai, A. W. Kahsay, C.-T. Chen, T. S. Zeleke, K. B. Ibrahim, C.-J. Huang, W.-N. Su, B.-J. Hwang, *Adv. Mater. Interfaces* **2018**, *5*.
[3] a) Q. Zhou, W. Zhang, M. Qiu, Y. Yu, *Materials Today Physics* **2021**, *20*; b) S. Nitopi, E. Bertheussen, S. B. Scott, X. Liu, A. K. Engstfeld, S. Horch, B. Seger, I. E. L. Stephens, K. Chan, C. Hahn, J. K. Norskov, T. F. Jaramillo, I. Chorkendorff, *Chem. Rev.* **2019**, *119*, 7610–7672.
[4] A. R. Woldu, Z. Huang, P. Zhao, L. Hu, D. Astruc, *Coord. Chem. Rev.* **2022**, *454*.
[5] A. N. Karaiskakis, E. J. Biddinger, *Energy Technol.* **2017**, *5*, 901–910.
[6] H. Shibata, J. A. Moulijn, G. Mul, *Catal. Lett.* **2008**, *123*, 186–192.
[7] a) C. Hahn, T. Hatsukade, Y. G. Kim, A. Vailionis, J. H. Baricuatro, D. C. Higgins, S. A. Nitopi, M. P. Soriaga, T. F. Jaramillo, *Proc. Natl. Acad. Sci. USA* **2017**, *114*, 5918–5923; b) K. J. P. Schouten, Z. Qin, E. Pérez Gallent, M. T. M. Koper, *J. Am. Chem. Soc.* **2012**, *134*, 9864–9867.
[8] A. J. Garza, A. T. Bell, M. Head-Gordon, *ACS Catal.* **2018**, *8*, 1490–1499.
[9] X. Feng, K. Jiang, S. Fan, M. W. Kanan, *J. Am. Chem. Soc.* **2015**, *137*, 4606–4609.
[10] Z. Chen, T. Wang, B. Liu, D. Cheng, C. Hu, G. Zhang, W. Zhu, H. Wang, Z.-J. Zhao, J. Gong, *J. Am. Chem. Soc.* **2020**, *142*, 6878–6883.
[11] A. D. Handoko, C. W. Ong, Y. Huang, Z. G. Lee, L. Lin, G. B. Panetti, B. S. Yeo, *J. Phys. Chem. C* **2016**, *120*, 20058–20067.
[12] Y. Katayama, F. Nattino, L. Giordano, J. Hwang, R. R. Rao, O. Andreussi, N. Marzari, Y. Shao-Horn, *J. Phys. Chem. C* **2018**, *123*, 5951–5963.
[13] I. V. Chernyshova, P. Somasundaran, S. Ponnurangam, *Proc. Natl. Acad. Sci. USA* **2018**, *115*, E9261–E9270.
[14] F. Scholten, K. C. Nguyen, J. P. Bruce, M. Heyde, B. Roldan Cuenya, *Angew. Chem. Int. Ed.* **2021**, *60*, 19169–19175.
[15] a) S. Popovic, M. Smiljanic, P. Jovanovic, J. Vavra, R. Buonsanti, N. Hodnik, *Angew. Chem. Int. Ed.* **2020**, *59*, 14736–14746; *Angew. Chem.* **2020**, *132*, 14844–14854; b) K. Van Daele, B. De Mot, M. Pupo, N. Daems, D. Pant, R. Kortlever, T. Breugelmans, *ACS Energy Lett.* **2021**, *6*, 4317–4327.
[16] S. J. Raaijman, N. Arulmozhi, M. T. M. Koper, *ACS Appl. Mater. Interfaces* **2021**, *13*, 48730–48744.
[17] W. Yang, K. Dastafkan, C. Jia, C. Zhao, *Advanced Materials Technologies* **2018**, *3*.
[18] a) Y. Lum, J. W. Ager, *Angew. Chem. Int. Ed.* **2018**, *57*, 551–554; *Angew. Chem.* **2018**, *130*, 560–563; b) B. Beverskog, I. Puigdomenec, *Journal of Electrochemical Society* **1997**, *144*.
[19] M. Raffi, S. Mehrwan, T. M. Bhatti, J. I. Akhter, A. Hameed, W. Yawar, M. M. ul Hasan, *Annals of Microbiology* **2010**, *60*, 75–80.
[20] Y. Hori, I. Takahashi, K. Osamu, N. Hoshi, *J. Phys. Chem. B* **2002**, *106*, 15–17.
[21] S. Vollmer, G. Witte, C. Wöll, *Catal. Lett.* **2001**, *77*.
[22] F. Calle-Vallejo, M. T. Koper, *Angew. Chem. Int. Ed.* **2013**, *52*, 7282–7285; *Angew. Chem.* **2013**, *125*, 7423–7426.
[23] Y. Jiang, J. T. Wang, Y. Wang, J. Yin, *Mater. Sci. Forum* **2016**, *850*, 857–863.
[24] X. Feng, K. Jiang, S. Fan, M. W. Kanan, *ACS Cent. Sci.* **2016**, *2*, 169–174.
[25] S. Trasatti, O. A. Petrii, *J. Electroanal. Chem.* **1992**, *327*, 353–376.
[26] P. Lobaccaro, M. R. Singh, E. L. Clark, Y. Kwon, A. T. Bell, J. W. Ager, *Phys. Chem. Chem. Phys.* **2016**, *18*, 26777–26785.
[27] a) H. Huang, H. Jia, Z. Liu, P. Gao, J. Zhao, Z. Luo, J. Yang, J. Zeng, *Angew. Chem. Int. Ed.* **2017**, *56*, 3594–3598; *Angew. Chem.* **2017**, *129*, 3648–3652; b) Y. Hori, H. Konishi, T. Futamura, A. Murata, O. Koga, H. Sakurai, K. Oguma, *Electrochim. Acta* **2005**, *50*, 5354–5369.

Manuscript received: April 21, 2022
Revised manuscript received: June 8, 2022
Version of record online: July 13, 2022